A Topographic View of Supercooled Liquids and Glass Formation

Frank H. Stillinger

Various static and dynamic phenomena displayed by glass-forming liquids, particularly those near the so-called "fragile" limit, emerge as manifestations of the multidimensional complex topography of the collective potential energy function. These include non-Arrhenius viscosity and relaxation times, bifurcation between the α- and β-relaxation processes, and a breakdown of the Stokes-Einstein relation for self-diffusion. This multidimensional viewpoint also produces an extension of the venerable Lindemann melting criterion and provides a critical evaluation of the popular "ideal glass state" concept.

Methods for preparing amorphous solids include a wide range of techniques. One of the most prominent, both historically and in current practice, involves cooling a viscous liquid below its thermodynamic freezing point, through a metastable supercooled regime, and finally below a "glass transition" temperature T_g. A qualitative understanding, at the molecular level, has long been available for materials produced by this latter preparative sequence; however, many key aspects of a detailed quantitative description are still missing. For-

The author is at AT&T Bell Laboratories, Murray Hill, NJ 07974, USA.

tunately, focused and complimentary efforts in experiment, numerical simulation, and analytical theory currently are filling the gaps.

The present article sets forth a descriptive viewpoint that is particularly useful for discussing liquids and the glasses that can be formed from them, although in principle it applies to all condensed phases. Conceptual precursors to this viewpoint can be found throughout the scientific literature (1), but most notably in the work of Goldstein (2). The objective here is to classify and unify at least some of the many static and kinetic phenomena associated with the glass transition.

Interaction Potentials

Condensed phases, whether liquid, glassy, or crystalline, owe their existence and measurable properties to the interactions between the constituent particles: atoms, ions, or molecules. These interactions are comprised in a potential energy function $\Phi(\mathbf{r}_1 \cdots \mathbf{r}_N)$ that depends on the spatial location $\mathbf{r}_i$ for each of those particles. The potential energy includes (as circumstances require) contributions from electrostatic multipoles and polarization effects, covalency and hydrogen bonding, short-range electron-cloud-overlap repulsions and longer range dispersion attractions, and intramolecular force fields. Obviously, the chemical characteristics of any substance of interest would substantially influence the details of Φ. Time evolution of the multiparticle system is controlled by the interactions, and for most applications of concern here the classical Newtonian equations of motion (incorporating forces specified by Φ) provide an adequate description of the particle dynamics.

In order to understand basic phenomena related to supercooling and glass formation, it is useful to adopt a "topographic" view of Φ. By analogy to topographic maps of the Earth's features, we can imagine a multidimensional topographic map showing the "elevation" Φ at any "location" $\mathbf{R} \equiv (\mathbf{r}_1 \cdots \mathbf{r}_N)$ in the configuration space of the N particle system. This simple change in perspective from conventional

three-dimensional space to a space of much higher dimension [$3N$ for structureless particles, and even more for particles that are asymmetric or nonrigid or both (3)] intrinsically creates no new information, but it facilitates the description and understanding of collective phenomena that operate in condensed phases, particularly in liquids and glasses.

An obvious set of topographic questions to ask concerns the extrema of the Φ surface, such as maxima ("mountain tops"), minima ("valley bottoms"), and saddle points ("mountain passes"). The minima correspond to mechanically stable arrangements of the N particles in space, with vanishing force and torque on every particle; any small displacement from such an arrangement gives rise to restoring forces to the undisplaced arrangement. The lowest lying minima are those whose neighborhoods would be selected for occupation by the system if it were cooled to absolute zero slowly enough to maintain thermal equilibrium; for a pure substance, this would correspond to a virtually perfect crystal. Higher lying minima correspond to amorphous particle packings and are sampled by the stable liquid phase above the melting temperature T_m (4).

Figure 1 shows a highly schematic illustration of the multidimensional "Φ-scape." Such a simplified representation can be misleading, but it serves to stress several key points. First, the minima have a substantial variation in depth and are arranged in a complex pattern throughout configuration space. Second, each minimum is enclosed in its own "basin of attraction," most simply defined as the set of all configurations in its "valley," that is, all locations that strict downhill motion would connect to that minimum. Third, contiguous basins share a boundary containing at least one saddle point, or transition state. Fourth, equivalent minima can be attained by permutations of identical particles. This last point implies, for a pure substance, that every minimum belongs to a group of $N!$ equivalent minima distributed regularly throughout the multidimensional configuration space.

An important issue concerning the Φ-scape topography that remains largely unresolved concerns the number of minima $\Omega(N)$, and in particular how fast it rises with N. Rather general arguments (bolstered by exact calculations for some special theoretical models) yield a simple generic form for the large-N limit in a single-component system (4, 5):

$$\Omega(N) \sim N! \exp(\alpha N) \qquad (1)$$

where $\alpha > 0$ depends significantly on the chemical nature of the substance considered. The permutational factor $N!$ has already been explained; the challenge is to predict α reliably from known molecular structures and interactions.

Melting and Freezing Criteria

The topographic view of the Φ-scape advocated above leads to a clean separation between the inherent structural aspects of the substance under consideration (that is, the classification of potential energy local minima), and the "vibrational" aspects that concern motions within and among the basins defined by those inherent structures. Such a separation leads naturally to a fresh examination of an old but very useful idea, namely, the Lindemann melting criterion for crystalline solids, first formulated in 1910 (6).

The Lindemann criterion concerns the dimensionless ratio, $\ell(T)$, of the root-mean-square (rms) vibrational displacement of particles from their nominal lattice positions, to the nearest-neighbor spacing a. It asserts that when temperature rise causes $\ell(T)$ to reach a characteristic instability value, melting occurs. X-ray and neutron diffraction experiments provide measurements of $\ell(T)$ (through the Debye-Waller factor) for a wide variety of real substances, and computer simulations can be used to calculate $\ell(T)$ for model systems. These results show that $\ell(T_m)$ varies a bit with crystal structure: It is approximately 0.13 for face-centered-cubic crystals and 0.18 for body-centered-cubic crystals (7). In any event, it is substantially constant across substances in a given crystal class and provides a good account of the pressure dependence of T_m for a given substance.

Vibrational motions contributing to $\ell(T_m)$ have a significant anharmonic character. But aside from a very small concentration of thermally created point defects in the crystal, these vibrations are confined to the basins surrounding the $N!$ absolute minima. At any temperature T, then, the Lindemann ratio for the crystal can be expressed:

$$\ell(T) = <(\Delta R)^2>^{1/2}/(Na) \qquad (2)$$

where ΔR is the intrabasin vibrational displacement from the absolute minimum in the multidimensional configuration space, and the brackets denote a thermal average confined to that basin at temperature T.

Although it is not obvious in the usual way of presenting the Lindemann melting criterion, Eq. 2 has a straightforward extension to the liquid phase. One simply recognizes that the thermal average and the displacements refer to inherent structures of the amorphous packing and their associated Φ-scape basins that predominate after melting. The mean nearest-neighbor distance a for the liquid phase (obtained from the measured radial distribution function) typically is close to that of the unmelted crystal.
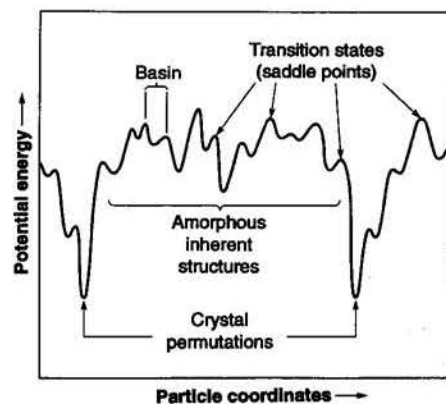
No laboratory experiment has yet been

Fig. 1. Schematic diagram of the potential energy hypersurface in the multidimensional configuration space for a many-particle system.
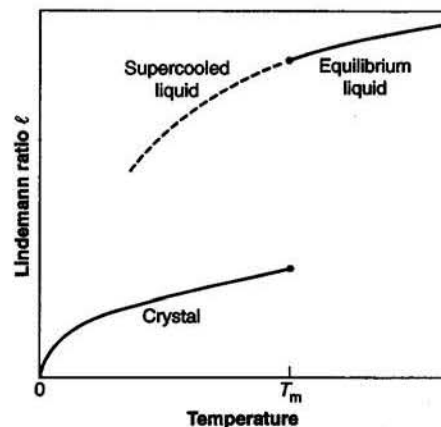

Fig. 2. Root-mean-square particle displacement divided by mean neighbor separation, versus temperature, for crystal and liquid phases. The value of this ratio for the crystal at the melting point, $\ell(T_m)$, is specified by the Lindemann melting criterion.

devised to measure $\ell(T)$ for liquids. Nevertheless, computer simulations for models of real substances can be designed to supply the needed information. Numerically, these simulations are required to generate a representative collection of system configurations for the temperature of interest and to evaluate the rms particle displacements that return each configuration to its corresponding inherent structure. Although only a small number of simulations of this kind have thus far been carried out (8), the main features of this extension are clear, and are summarized qualitatively in Fig. 2. The crystal and liquid $\ell(T)$ curves are distinct; both monotonically increase with T, with the curve for the liquid located well above that for the crystal. At the melting-freezing point, ℓ_{liq} is approximately three times that for the crystal; equivalently, the rms particle displacement is approximately one-half that of the nearest-neighbor spacing.

In its conventional form, the Lindemann criterion advances an asymmetric, one-
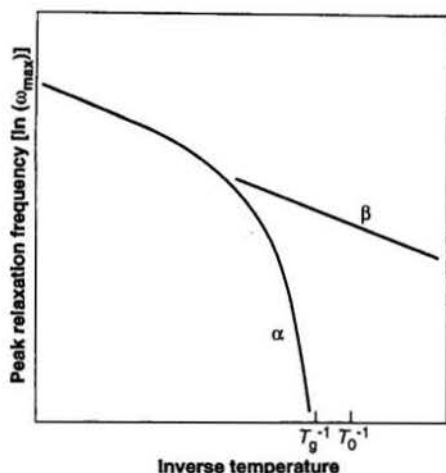
Fig. 3. Temperature dependence of peak relaxation (or absorption) frequencies for glass-forming liquids.

phase view of the first-order crystal-liquid transition. This model contrasts markedly with the thermodynamic description that calls for two-phase equality of pressure and chemical potential at the transition. However, the extension just described effectively restores two-phase symmetry. It supplements the melting criterion with an exactly analogous Lindemann-like freezing criterion for the liquid, specifically, that thermodynamic instability with respect to freezing occurs when cooling causes $\ell_{liq}(T)$ to decline to the cited transition value.

Although it is relatively difficult to superheat crystals above their T_m, supercooling of the melt is commonplace, particularly with viscous liquids. Figure 2 shows the extension of $\ell_{liq}(T)$ into the $T < T_m$ regime of supercooling, under the assumption that crystal nucleation has been avoided. In this extension, the system's configuration point $R(t)$ continues to wander as time t progresses among the basins for amorphous inherent structures, without discovering entrance channels to any of the absolute-minimum basins of the crystalline state. Upon cooling to absolute zero, the system becomes trapped almost at random in one of these inherent-structure basins of the amorphous state, ℓ_{liq} becomes small (vanishing for classical statistics), and the system becomes a rigid glass.

Arrested Kinetics

The entire collection of $\Omega(N)$ basins can be classified by their depths. Let $\phi \equiv \Phi/N$ denote the inherent-structure potential energy for any given basin on a per-particle basis. In analogy to Eq. 1 above, it can be shown that the distribution of basins by depth has the form $N!\exp[\sigma(\phi)N]$ in the large-N limit (5). A mean vibrational free energy per particle, f_v, can then be defined for basins of depth ϕ. The equilibrium state

of the system at temperature T corresponds to preferential occupation of basins with depth $\phi^*(T)$, which is the ϕ value that maximizes the simple combination (5, 9):

$$\sigma(\phi) - (k_B T)^{-1}[\phi + f_v(\phi, T)] \qquad (3)$$

where k_B is Boltzmann's constant. When T is near T_m, this combination has two local maxima with respect to ϕ; the first-order melting transition corresponds to a discontinuous change in ϕ^* as the role of the absolute maximum switches from one to the other at T_m.

Supercooling the liquid phase below T_m kinetically avoids switching back to deep crystalline basins, but rather the liquid remains in those that correspond to the other local maximum of Eq. 3, given by $\phi^*_{liq}(T)$, that continues to refer to higher lying amorphous inherent structures. So long as the system configuration point $R(T)$ can move more or less freely among the higher lying amorphous inherent structures and attain a representative sampling while avoiding crystal nucleation, the system remains in a reproducible quasi-equilibrium state of liquid supercooling (9).

The individual transitions that carry the system between contiguous (boundary-sharing) basins apparently almost always involve localized particle rearrangements. In other words, only order $O(1)$ out of N of the particles undergo substantial location shifts. This is true whether the basins are those for substantially crystalline inherent structures (and the transition involves creation or destruction of point defects), or whether they refer to a pair of amorphous packings. Consequently, the activation barrier that must be surmounted, and the final change in basin depth will also only be $O(1)$. Because the total kinetic energy is much larger (roughly $Nk_B T$), enough thermal energy is virtually always available in principle to surmount the intervening barrier. The bottleneck is that this kinetic energy is distributed throughout the many-particle system, and it may take a very long time for a proper fluctuation to concentrate enough kinetic energy at the required location to effect the transition between basins.

Relaxation response functions in the time domain, $g_v(t)$, to any of a variety of weak external perturbations v (mechanical, electrical, thermal, optical, and so forth) provide an indication of the actual restructuring kinetics resulting from interbasin transitions. If the assumption that the initial-time normalization $g_v(0) = 1$ is imposed, the areas under the $g_v(t)$ curve along the positive time axis define mean relaxation times $\tau_v(T)$. These depend somewhat on property v, but in supercooled liquids they tend to display essentially a common rapid rise with declining temperature and can often be fitted to a Vogel-Tammann-

Fulcher (VTF) form (10):

$$\tau_v(T) \cong \tau_0 \exp[A/(T - T_0)] \qquad (4)$$

where τ_0 is in the picosecond range and A and T_0 are positive constants.

So long as all τ_v are substantially shorter than the time available for experimental measurement, the supercooled liquid remains in a state of quasi-equilibrium, and in particular inhabits and moves among basins whose depths are closely clustered around $\phi^*_{liq}(T)$. But as T declines, the mean relaxation times represented by the VTF form increase strongly and all cross the time scale of experimental measurement at essentially a common glass transition temperature $T_g > T_0$. Further reduction in T fails to lower the depth of the inhabited basins below $\phi^*_{liq}(T_g)$. The supercooled liquid then has fallen out of quasi-equilibrium. The ratio T_g/T_m for most good glass-forming liquids falls in the range from 0.60 to 0.75.

Careful examination of the relaxation functions $g_v(t)$ above T_g reveals the presence of distinct processes. At very short times (comparable to vibrational periods), intrabasin relaxation predominates. This domain is followed by a much more extended time regime during which interbasin structural relaxation processes occur, and in the long-time limit of this regime the relaxation inevitably seems to display a Kohlrausch-Williams-Watts (KWW) "stretched exponential" decay (11):

$$g_v(t) \sim \Gamma_v \exp[-(t/t_v)^\theta] \qquad (5)$$

in which $0 < \theta \leq 1$ and Γ_v is a constant; the characteristic time t_v is comparable to mean relaxation time τ_v when T is near T_g.

The $\theta = 1$ limit in Eq. 5 corresponds to simple Debye relaxation, with t_v serving as the single structural relaxation time. However, smaller θ values lead to a broad distribution of relaxation times, and by transforming g_v to the frequency domain this breadth becomes explicit (12). Peaks in the frequency-dependent absorption then correspond approximately to the dominant relaxation times.

As Fig. 3 illustrates, the temperature dependence of peak relaxation frequency for liquids often exhibits a bifurcation (13). In the equilibrium liquid range and into the moderately supercooled regime, there is a single absorption maximum frequency. Upon approaching T_g, this peak splits into a pair of maxima, the slow α ("primary") and faster β ("secondary") relaxations. The former are non-Arrhenius and kinetically frozen out at T_g, and the latter are more nearly Arrhenius and remain operative at T_g.

The α, β relaxation bifurcation has a straightforward interpretation in terms of the Φ topography. As T declines, the configuration point $R(t)$ is forced into regions of increasingly rugged and heterogeneous

topography in order to seek out the ever deeper basins that are identified by $\phi_{liq}^*(T)$. The lower the temperature, the rarer and more widely separated these basins must be. However, the elementary transition processes that connect contiguous basins continue to require only local rearrangements of small numbers of particles. Evidently, the basins are geometrically organized to create a two-scale length and potential energy pattern; Fig. 4 illustrates this feature.

The β processes are identified with the elementary relaxations between neighboring basins, whereas the α processes entail escape from one deep basin within a large-scale "crater" or "metabasin" and eventually into another (14). Because the latter requires a lengthy directed sequence of elementary transitions, it will acquire a net elevation change (activation energy) many times that of the former. Also, the vast intervening stretch of higher lying basins produces a large activation entropy.

Viscosity and Self-Diffusion

The relaxational response of a fluid to shear stress is often described by a specific instance of Eq. 4, the Maxwell relaxation time $\tau_M(T)$, defined by the ratio of the shear viscosity $\eta(T)$ to the elastic modulus G, which is nearly temperature independent. Consequently, the VTF form in Eq. 4 is also a useful representation of shear viscosity [indeed, this was its original application (10)]:

$$\eta(T) \cong \eta_0 \exp[B/(T - T_0)] \qquad (6)$$

with virtually the same divergence temperature T_0 that obtains for other types of relaxation. Experimentally, T_g's often correspond to η in the range from 10^{11} to 10^{13} poise for nonpolymeric liquids.

The VTF representation for viscosity generates a useful classification of glass-forming liquids between "strong" and "fragile" extremes (15), depending on the value of the ratio T_0/T_m (or alternatively T_0/T_g). The strong limit has $T_0/T_m \cong 0$, and $\eta(T)$ displays Arrhenius temperature behavior; real material examples that appear to be close to this limit are the oxide glasses SiO_2 and GeO_2. The fragile limit displays dramatic non-Arrhenius $\eta(T)$, and is illustrated by orthoterphenyl, and the ionic material $K_{0.6}Ca_{0.4}(NO_3)_{1.4}$.

The variation in behavior between the strong and fragile extremes can be traced back to topographic differences in the Φ-scapes for the respective materials. The extreme limit of strong glass formers presents a uniformly rough (single energy scale) topography, in which only the β transitions of Fig. 4 have relevance. Little or no coherent organization of the individual basins into large and deep craters, associated with the low-temperature α transitions, appears to be
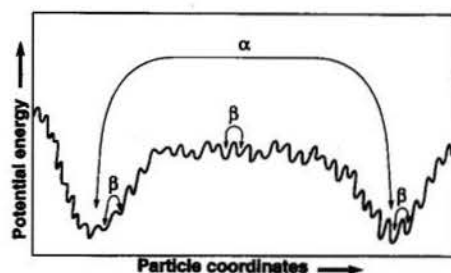

Fig. 4. Two-scale potential energy topography characteristic of regions of configuration space explored by fragile glass formers near T_g. The elementary interbasin transitions are associated with β relaxations, and large distance intercrater transitions are associated with α relaxations.

present. It is no surprise then that the α,β bifurcation is weak or absent in the strong cases. In contrast, the most fragile glass formers indeed exhibit significant Φ-scape cratering and distinctive α,β bifurcation. The relatively large effective singularity temperature T_0 for fragile materials reflects the larger and wider net barriers that they must surmount, as T declines toward T_0, for the system configuration to pass from the interior of one inhabited crater to another of comparable or greater depth.

The self-diffusion constant D measures the rate of increase with time, because of Brownian motion, of the mean square displacement of a tagged particle in the medium. The Stokes-Einstein relation connects D to η and to an effective hydrodynamic radius b for the particle:

$$D(T) = k_B T/[6\pi b\eta(T)] \qquad (7)$$

(the constant 6π assumes a "sticking" boundary condition at the particle surface). This relation has been remarkably successful at correlating independent measurements of $D(T)$ and $\eta(T)$ for many liquids as both vary over many orders of magnitude in the stable and supercooled liquid regimes. However, some recent experiments on fragile glass formers near T_g show a striking breakdown of Eq. 7; in these cases $D(T)$ becomes two orders of magnitude or more larger than the measured $\eta(T)$ would indicate (16). Paradoxically, this dramatic effect occurs while the corresponding rotational diffusion rate is still linked to $\eta(T)$ or only weakly decoupled (17).

Once again, the Φ-scape cratering characteristic for fragile glass formers offers an explanation. When the temperature is low and the system configuration point emerges from one deep crater to search for another, it has been emphasized that a long sequence of elementary interbasin transitions will be involved. In three dimensions, this sequence would appear as a local structural excitation running around in a microscopic domain that encompasses many particles, temporarily fluidizing that domain com-
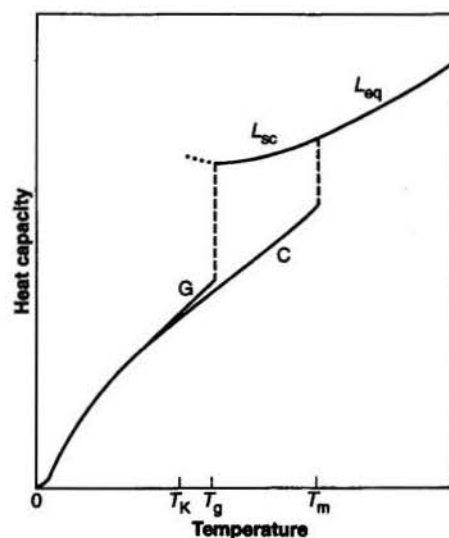

Fig. 5. Typical heat capacity curves for fragile glass formers in crystal (C), supercooled liquid (L_{sc}), equilibrium liquid (L_{eq}), and glass (G) phases; T_K is the Kauzmann temperature.

pared to the surroundings. Because such domains are expected to be large on the molecular scale near T_g and to have long lifetimes, translational diffusion receives a disproportionate enhancement compared to rotational diffusion, and a detailed analysis (18) shows that the latter continues to adhere more closely than the former to the temperature dependence of $\eta(T)$.

Ideal Glass State?

Figure 5 illustrates schematically variation with temperature of the heat capacity (C_p, constant pressure) typically observed for fragile glass formers. Notable features are: (i) C_p rises discontinuously when the crystal melts at T_m; (ii) supercooling the liquid down toward T_g increases the discrepancy between C_p (liquid) and C_p (crystal); and (iii) further cooling produces a nearly discontinuous drop in C_p (liquid) so that C_p (glass) is very close to that of C_p (crystal) at the same low temperature. In view of the basin-trapping interpretation of the glass transition, it can be concluded that the intrabasin vibrational properties are largely the same for all basins, whether corresponding to crystalline or to amorphous inherent structures. Furthermore, most of the enhancement of C_p (liquid) over C_p (crystal) above T_g stems from the temperature variation of ϕ_{liq}^*, the depth of the basins predominately inhabited by the supercooled liquid.

The latent heat of melting causes the liquid at T_m to possess a substantially higher entropy than the crystal. However, the C_p discrepancy illustrated in Fig. 5 means that the liquid loses entropy faster than the crystal as both are cooled below T_m. The strongly supercooled liquid at T_g still has the higher

entropy, although the difference has been substantially reduced. Smooth extrapolation of C_p (liquid) below T_g and of the corresponding entropy indicate the existence of a positive "Kauzmann temperature" T_K at which the crystal and the extrapolated liquid attain equal entropies (19). Considering that vibrational entropies are nearly the same for the two phases, and that the inherent structural entropy of the ordered crystal vanishes, the fully relaxed glass at T_K (the extrapolated liquid) must also have vanishing inherent structural entropy. This realization, coupled with the empirical observation that $T_K \cong T_0$, the mean relaxation-time divergence temperature, has generated the concept of an "ideal glass state" that could be experimentally attained if only sufficiently slow cooling rates were available (20).

If indeed it exists, the ideal glass state must correspond to the inherent structure with the lowest potential energy (deepest "crater") that is devoid of substantial regions with local crystalline order. Unfortunately, the details of this noncrystallinity constraint are unclear but may be crucial: Qualifying inherent structures may depend on the maximum size and degree of perfection permitted crystalline inclusions in otherwise amorphous structures. This ambiguity, or non-uniqueness of choice criterion, would seem to undermine the concept of a substantially unique ideal glass state.

It has also been argued (9) that the seemingly innocuous extrapolations that identify a positive Kauzmann temperature T_K (and by implication T_0) are flawed. Localized particle rearrangements (associated with β relaxations) are always possible, even in a hypothetical ideal glass structure, and raise the potential energy only by $O(1)$. These structural excitations in the strict sense prevent attaining the ideal glass state at positive temperature, in conflict with the usual view (20).

In spite of these formal reservations, the ideal glass state concept remains valuable. Careful and systematic experiments on the most fragile glass formers should help to remove some of the obscuring uncertainties.

Conclusions

By focusing attention on the topographic characteristics of Φ in the multidimensional configuration space, a comprehensive description becomes available for static and kinetic phenomena exhibited by supercooled liquids and their glass transitions. In particular, this viewpoint rationalizes the characteristic properties of fragile glass formers, including non-Arrhenius viscosity, primary-secondary relaxation bifurcation, and the enhancement of self-diffusion rates over the Stokes-Einstein prediction. This multidimensional topographic representa-

tion has the further benefit of uncovering and promoting several basic research topics that need sustained experimental and theoretical-simulational attention. Examples of the latter are the material-specific enumeration of inherent structures (Φ minima), the exploitation of the Lindemann-like freezing criterion for liquids and its relation to the glass transition, and the critical evaluation of the ideal-glass-state concept.

REFERENCES AND NOTES

1. J. D. Bernal, *Nature* **183**, 141 (1959); H. Eyring *et al.*, *Proc. Natl. Acad. Sci. U.S.A.* **44**, 683 (1958); M. R. Hoare, *Adv. Chem. Phys.* **40**, 49 (1979).
2. M. Goldstein, *J. Chem. Phys.* **51**, 3728 (1969); *ibid.* **67**, 2246 (1977).
3. For constant-pressure circumstances, system volume becomes an additional coordinate and Φ includes a pressure-volume contribution PV.
4. F. H. Stillinger and T. A. Weber, *Science* **225**, 983 (1984).
5. _____, *Phys. Rev. A* **25**, 978 (1982).
6. F. A. Lindemann, *Z. Phys.* **11**, 609 (1910).
7. H. Löwen, *Phys. Rep.* **237**, 249 (1994).
8. R. A. LaViolette and F. H. Stillinger, *J. Chem. Phys.* **83**, 4079 (1985).
9. F. H. Stillinger, *ibid.* **88**, 7818 (1988).
10. G. W. Scherer, *J. Am. Ceram. Soc.* **75**, 1060 (1992).
11. K. L. Ngai, Comments *Solid State Phys.* **9**, 127 and 141 (1979); R. Böhmer, K. L. Ngai, C. A. Angell, D. J. Plazek, *J. Chem. Phys.* **99**, 4201 (1993).
12. E. W. Montroll and J. T. Bendler, *J. Stat. Phys.* **34**, 129 (1984).
13. G. P. Johari and M. Goldstein, *J. Chem. Phys.* **53**, 2372 (1970).
14. F. H. Stillinger, *Phys. Rev. B* **41**, 2409 (1990).
15. C. A. Angell, in *Relaxations in Complex Systems*, K. Ngai and G. B. Wright, Eds. (National Technical Information Service, U.S. Department of Commerce, Springfield, VA, 1985), p. 1.
16. F. Fujara, B. Geil, H. Sillescu, G. Fleischer, *Z. Phys. B* **88**, 195 (1992); M. T. Cicerone and M. D. Ediger, *J. Phys. Chem.* **97**, 10489 (1993); R. Kind *et al.*, *Phys. Rev. B* **45**, 7697 (1992).
17. M. T. Cicerone, F. R. Blackburn, M. D. Ediger, *J. Chem. Phys.* **102**, 471 (1995).
18. F. H. Stillinger and J. A. Hodgdon, *Phys. Rev. E* **50**, 2064 (1994).
19. W. Kauzmann, *Chem. Rev.* **43**, 219 (1948).
20. J. Jäckle, *Rep. Prog. Phys.* **49**, 171 (1986).